ESTIMATING LUMBER PROPERTIES WITH ACOUSTIC-BASED TECHNOLOGIES—PART 1: MODELING ACOUSTIC (STRESS) WAVE BEHAVIOR IN CLEAR WOOD AND LUMBER[1]

Christopher Adam Senalik†

Research General Engineer
USDA Forest Products Laboratory
Madison, WI 53726
E-mail: christopher.a.senalik@usda.gov

*F. J. N. França**

Assistant Research Professor
E-mail: fn90@msstate.edu

R. D. Seale

Warren S. Thompson Professor
Department of Sustainable Bioproducts
Mississippi State University
Mississippi State, MS 39762-5724
E-mail: rds9@msstate.edu

Robert J. Ross

Supervisory Research General Engineer
USDA Forest Products Laboratory
Madison, WI 53726
E-mail: rjross@fs.fed.us

R. Shmulsky†

Warren S. Thompson Professor and Department Head
Department of Sustainable Bioproducts
Mississippi State University
Mississippi State, MS 39762-5724
E-mail: rs26@msstate.edu

(Received March 2020)

Abstract. This research article summarizes results from Part 1 of a study designed to examine using advanced signal processing techniques with acoustic-based lumber assessment technologies to evaluate the MOE, ultimate tension stress (UTS), and MOR of structural lumber. In Part 1 of this research article, a mathematical model of acoustic wave behavior in an idealized specimen is derived using fundamental mechanics. Published information on the physical and mechanical properties of clear, defect-free wood is input into the model to examine acoustic wave behavior. Wave behavior is then examined experimentally in a series of wood specimens. Observed wave behavior in the clear wood specimens, in both time and frequency domains, closely resembles idealized wave behavior. In Part 2 of this research article, predictions from the model are used to improve estimation of the UTS of wood specimens.

Keywords: Wave model, frequency, clear wood, lumber, modulus of elasticity.

* Corresponding author
† SWST member

INTRODUCTION

Wood is a biological material with inherent variation and internal features, which may not always be visible on the exterior. The collection of the sample has the goal of creating a continuous range of tension strength values from low to high. A particularly dense piece of wood, with a high number of rings per centimeter, that contains a knot may have higher tension strength than a defect-free piece, that is, low density with a low number of rings per centimeter. The presence or absence of defects does not necessarily give an insight into the ultimate tension strength of an individual piece. In Part 1 of this study, a model is developed to aid in identifying relevant characteristics. In Part 2, the ultimate tension stress (UTS) is estimated from characteristics of the time and frequency domains. The goal of the entire study was to accurately assess the tensile strength of the wood.

Various nondestructive methods are currently used to evaluate, sort, and grade structural lumber. At its core, the purpose of strength grading is to sort lumber into categories which have known minimum characteristics. Lumber is also graded for appearance and usefulness characteristics. Evaluation of visual characteristics of a piece of lumber is arguably the most widely used nondestructive evaluation technique in the forest products industry. At present, all lumber grading requires the evaluation of visual characteristics. This may be accomplished by human graders and/or various scanning techniques. Even mechanically graded lumber has visual characteristics required to be placed into a grade, regardless of any stiffness or strength determination. Characteristics such as the size, number, and location of knots are just one of several common visual characteristics considered when grading lumber.

Ross (2015) summarized a wide range of research that use physical and mechanical characteristics to grade lumber. From this research, rugged, commercially available lumber grading machines were developed. One technology currently in use is based on measurement of the acoustic properties of a lumber specimen. Specifically, the speed at which a mechanically induced acoustic wave flows along the length of a specimen is measured. The wave speed along with the lumber density is used to determine the MOE. The MOE, in turn, is used to estimate the MOR in bending and UTS parallel to the grain. Unfortunately, the MOE currently accounts for only 50-55% of the variation in the MOR or UTS, and additional factors are needed for estimation of lumber strength. This information, along with certain visually identified characteristics, is used to assign a grade to the lumber. The combination of nondestructive testing and visual grading leads to more accurate estimations of the lumber strength, allowing wiser use of the lumber resources.

The flow of an acoustic wave in a lumber specimen is influenced by a variety of factors, such as the size, number, and location of knots; slope of grain; presence decay; and many others. It is widely accepted that these factors have an influence on the MOE and MOR of lumber (Ross 2010). The measurement system which determines the MOE yields an electronic signature that contains additional information regarding the movement of an acoustic wave in a lumber specimen. Although a significant number of published research findings exist on the measurement and use of the acoustic-based MOE for evaluating lumber and other wood products (Senalik et al 2014; Ross 2015), little more than cursory information is published on the effects that naturally occurring characteristics have on acoustic wave behavior in lumber and the potential impact these have on evaluating lumber strength.

The objectives of this research were to 1) examine fundamental acoustic wave behavior in clear wood and lumber, 2) explore the effect that naturally occurring defects such as knots have on acoustic wave behavior in lumber, and 3) investigate the possibility of using advanced signal processing techniques to enhance acoustic-based lumber processing. Item 1 was addressed in this article. Items 2 and 3 are addressed in Part 2 of this research.

The study begins with an examination of the theoretical foundation of acoustic wave behavior

in an idealized homogeneous viscoelastic bar of similar thickness and length to that of a lumber specimen. A review of published research on acoustic wave behavior in clear wood and lumber specimens is conducted, including published works that examined the effects that naturally occurring characteristics (such as knots) have on wave behavior. Laboratory tests are then conducted on a sample of lumber specimens, and advanced signal processing techniques are used to analyze acoustic wave signatures obtained.

Longitudinal Wave Behavior in Wood

Given that the public needs safe, reliable, and available building materials, historically, assumptions about lumber homogeneity and isotropic structure have been made in an effort to build reliable, fast, prediction models. However, wood is orthotropic, so wave motion through wood is different from that through isotropic, homogeneous materials (Senalik 2013). Several studies were conducted to examine wave behavior in wood. Bertholf (1965) conducted an evaluation of the basic wave theory and its applicability to small, clear wood specimens. He verified predicted stress wave behavior with strain wave measurements and verified the dependence of wave propagation velocity on the MOE of clear wood. Galligan and Bertholf (1963) used 1.9 × 1.9 × 76.2-cm clear wood specimens in a study designed to examine the use of piezoelectric properties to examine wave behavior. They compared measurements of dynamic strain wave patterns made using strain gauges and piezoelectric probes and observed similar results. They also examined the relationship between the dynamically measured MOE vs MOE obtained from compression tests parallel to the fiber axis. A strong linear relationship was observed through graphical representation of the data, but no coefficient of determination (r^2) value was given.

Galligan and Courteau (1965) and Pellerin and Galligan (1973) found that the MOE, as determined by measuring the propagation velocity of induced stress waves, could be used to predict the static bending MOE of lumber specimens. They used a small sample size of 40 pieces of structural lumber in their experiment and obtained an excellent correlation between modulus values, with a coefficient of determination (r^2) of 0.914.

Theoretical Foundation

Longitudinal wave behavior in an idealized viscoelastic bar: qualitative analysis. For the purpose of discussion, researchers consider a long, thin viscoelastic bar that is subjected to a repeatable impact force at its end for a very short period of time. As a result of the impact, a zone exists at the end of the bar in which the particles of the bar are moving relative to it. This zone, or wave, immediately begins along the length of the bar as particles at the leading edge of the wave become excited. At the same time, particles at the trailing edge of the wave come to rest. Hence, the wave moves along the length of the bar at a constant speed, but its individual particles have only small longitudinal movement as a result of the wave passing over them (Graff 1975).

After traveling the length of the bar, this forward moving wave impinges on the free end of the bar, is reflected, and begins returning along the length of the bar. Movement of the particles resulting from this backward moving wave is in the same direction as that of the forward moving wave because the particles are now subjected to a tensile force, rather than a compressive one. Consequently, for a forward moving compressive wave, both particle motion and wave propagation are in the same direction, whereas for a tensile wave particle, motion is opposite to the direction of propagation. Energy is dissipated as the wave travels along the length of the bar, and with each successive pass, the wave particle motion diminishes. Eventually, all particles within the bar come to rest (Graff 1975). In practice, the energy loss takes the form of attenuation of the measured signal.

Development of a mathematical model. Figure 1 shows the unrestrained prismatic bar of length L with a typical segment of infinitesimal length dx

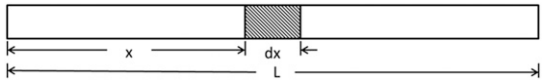

Figure 1. (a) Theoretical longitudinal vibration of a prismatic bar, generated using physical and mechanical property data for loblolly pine and Eq 18. Time domain with nine harmonics of the fundamental frequency. (b) Frequency-domain analysis showing the relative magnitude of each harmonic.

located at a distance x from its left end. In the following derivation, it is assumed that cross sections of this bar remain plane and that particles in every cross section moved only in the x direction. The longitudinal extensions and contractions that take place during such a vibration are accompanied by some small lateral deformations. However, in the following discussion, it is assumed that the length of the longitudinal waves is large in comparison with the lateral dimensions of the bar. In this case, the effect of lateral displacements on the longitudinal motions can be neglected without substantial error (Ross 1984).

Let $u(x,t)$ denote the longitudinal displacement of the point on the bar's cross section at "x." When the bar vibrates longitudinally, the axial forces on the differential segment "dx" are as shown in Fig 2 summed to yield the following equation:

$$\frac{\partial S}{\partial x}dx - \rho \cdot A \cdot \frac{\partial^2 u}{\partial t^2}dx = 0, \tag{1}$$

where S is the internal axial force resultant on the bars' cross section at x, ρ is the mass density of the material, A is the cross-sectional area of the bar, and $\frac{\partial^2 u}{\partial t^2}$ is the particle acceleration.

Using the following stress–strain relationship (Graff 1975) to represent the viscoelastic behavior of the material,

$$\sigma_x = E \cdot \varepsilon_x + \bar{c} \cdot \dot{\varepsilon}_x, \tag{2}$$

where σ_x is the axial stress, E is the MOE, $\varepsilon_x = \frac{\partial u}{dx}$ is the axial strain, and $\bar{c}$ is the internal damping coefficient,

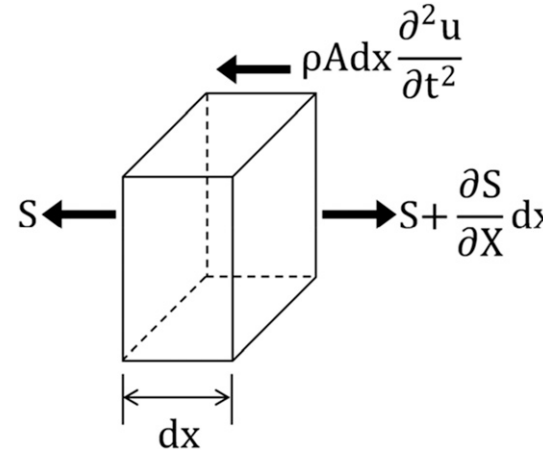

Figure 2. Comparison of MOE and fundamental frequencies from acoustic wave measurement and static testing. (a) Dynamic MOE vs tension MOE. (b) Fundamental frequencies predicted by the model given in Eq 18 vs those taken from acoustic signals during testing.

$$\dot{\varepsilon}_x = \frac{\partial \varepsilon_x}{\partial t}.$$

The axial force S is expressed in terms of the axial stress σ_x as follows:

$$S = \int_0^L \sigma_x dA = [E \cdot \varepsilon_x + \bar{c} \cdot \dot{\varepsilon}_x] \cdot A. \tag{3}$$

S is then expressed in terms of the axial strain as follows:

$$S = \left[E \cdot \frac{\partial u}{\partial x} + \bar{c} \cdot \frac{\partial^2 u}{\partial x \partial t} \right] \cdot A \tag{4}$$

which when substituted into Eq 1 yields the following differential equation of motion:

$$\frac{E}{\rho}\frac{\partial^2 u}{\partial x^2} + \frac{\bar{c}}{\rho} \cdot \frac{\partial^2 u}{\partial x \partial t} = \frac{\partial^2 u}{\partial t^2} \tag{5}$$

General solution. It is assumed that the general solution of Eq 5 is the following form:

$$u(x,t) = X(x)\cdot T(x). \tag{6}$$

Substituting Eq 6 into Eq 5 yields the following equation:

$$\left[\frac{E}{\rho} + \frac{\bar{c}}{\rho}\cdot\frac{\partial}{\partial t}\right]\cdot X''(x)\cdot T(t) = X(x)\cdot \ddot{T}(t), \tag{7}$$

where $X''(x) = \dfrac{\partial^2 X}{\partial x^2}$ and $\ddot{T}(t) = \dfrac{\partial^2 T}{\partial t^2}$

which after rearranging yields the following equation:

$$\frac{\ddot{T}(t)}{\left[\dfrac{E}{\rho}\cdot T(t) + \dfrac{\bar{c}}{\rho}\cdot \dot{T}(t)\right]} = \frac{X''(x)}{X(x)}, \tag{8}$$

where $\dot{T}(t) = \dfrac{\partial T}{\partial t}$.

Because the left-hand side of Eq 8 is a function of "x" only and the right-hand side is a function of "t" alone, each side must be equal to a constant.

Letting.

$$\frac{\ddot{T}(t)}{\left[C^2\cdot T(t) + \dfrac{\bar{c}}{\rho}\cdot \dot{T}(t)\right]} = \frac{X''(x)}{X(x)} = -\frac{\omega^2}{C^2}, \tag{9}$$

where $C = \sqrt{\dfrac{E}{\rho}}$ and is the longitudinal wave velocity.

Two ordinary differential equations are written from Eq 9. Those equations are given in Eqs 10 and 11a. The subscript "i" refers to harmonics of the fundamental frequency.

$$X_i'' + \frac{\omega_i^2}{C^2}\cdot X_i = 0 \tag{10}$$

$$\ddot{T}_i + \frac{\bar{c}}{\rho}\cdot\frac{\omega_i^2}{C^2}\dot{T}_i + \omega_i^2 T_i = 0 \tag{11a}$$

The solution of Eq 10 is given as follows:

$$X_i = b_{1i}\cdot\cos\frac{\omega_i\cdot x}{C} + b_{2i}\cdot\sin\frac{\omega_i\cdot x}{C}. \tag{12}$$

Eq 11a is simplified by defining a variable, α, as given follows:

$$\alpha_i = \frac{\bar{c}\omega_i^2}{2\cdot E}$$

$$\ddot{T}_i + 2\alpha_i\cdot\dot{T}_i + \omega_i^2\cdot T_i = 0 \tag{11b}$$

Whose solution is as follows:

$$T_i = e^{-\alpha_i t}(a_{1i}\cdot\cos\beta_i t + a_{2i}\cdot\sin\beta_i t), \tag{13}$$

where $\beta_i = \sqrt{\omega_i^2 - \alpha_i^2}$.

Substituting Eqs 12 and 13 into Eq 6 yields the following equation:

$$u(x,t) = \sum_{i=0}^{\infty} e^{-\alpha_i t}(a_{1i}\cdot\cos\beta_i t + a_{2i}\cdot\sin\beta_i t) \cdot\left(b_{1i}\cdot\cos\frac{\omega_i\cdot x}{C} + b_{2i}\cdot\sin\frac{\omega_i\cdot x}{C}\right) \tag{14}$$

which is the general expression for the free longitudinal vibration of a uniform viscoelastic bar. For a bar with free–free boundary conditions, the strain at the end of the bar must equal zero.

$$\frac{\partial u(x,t)}{\partial x} = 0 \text{ at } x = 0, L,$$

where L is the length of the bar.

$$\frac{\partial u(x,t)}{\partial x} = \sum_{i=0}^{\infty} e^{-\alpha_i t}(a_{1i}\cdot\cos\beta_i t + a_{2i}\cdot\sin\beta_i t) \cdot\left(-b_{1i}\cdot\sin\frac{\omega_i\cdot x}{C} + b_{2i}\cdot\cos\frac{\omega_i\cdot x}{C}\right) \tag{15}$$

At x equal to zero, the sine term that is a function of x becomes zero and the cosine term becomes one; therefore, b_{2i} must be zero. At x equal to L (the length of the bar), for the sine term to go to zero without a trivial solution (i.e., $b_{1i} = 0$), the term ω_i takes the form of Eq 16.

$$\omega_i = \frac{n_i \pi C}{L}, \tag{16}$$

where n_i is a nonnegative integer ($n_0 = 0$, $n_1 = 1$, $n_2 = 2$, $n_3 = 3\ldots$).

At time equal to zero, the displacement at all points along the bar must be equal to zero; therefore, a_{1i} must be equal to zero.

$$u(x,t) = \sum_{i=0}^{\infty} e^{-\alpha_i t}(a_{2i} \cdot \sin\beta_i t) \cdot \left(b_{1i} \cdot \cos\frac{n_i \pi \cdot x}{L}\right) \tag{17}$$

By defining D_i as the product of a_{2i} and b_{1i}, Eq 17 is simplified to an expression with a single unknown. The expression is shown in Eq 18 (Ross 1984).

$$u(x,t) = \sum_{i=0}^{\infty} D_i \cdot e^{-\alpha_i t} \cdot \sin\beta_i t \cdot \cos\frac{n_i \pi \cdot x}{L} \tag{18}$$

MATERIALS AND METHODS

The specimens in the experimental phase of this study are cut from a sample of visually graded number 2 (No. 2), southern pine 38 × 184-mm lumber (nominal 2 × 8 in). From the lumber, 103 38 × 38 × 2438-mm specimens are cut as shown in Fig 3. The specimens are conditioned to approximately 12% EMC before testing in a room kept at constant conditions of 21°C and 65% RH. The dimensions and weight of each specimen are measured before testing. Specimens are selected based on visual inspection with the goal of obtaining a wide range of characteristics. The sample included several specimens that are visually free from significant strength-reducing characteristics, including knots. Other specimens contained large knots. The specimens were not segregated according to whether they contained defects; the reason for this decision is explained in the Results section.

The experimental setup is illustrated in Fig 4. To insulate the specimen from external vibrations, supports made of ethylene–vinyl acetate foam rubber are used. A pendulum with a 5-g lead mass is used as an excitation system. The pendulum is raised to a height of 15 cm during all tests to ensure the same potential energy for all specimens. The longitudinal vibration waves that traveled through the piece are recorded. The fundamental frequency of each of the 103 specimens is determined from the frequency domain of each recorded signal.

The time-domain signal from each specimen is recorded, and Fourier transformation is performed to observe the frequency-domain spectrum. The dynamic MOE (MOE_D) of each piece is calculated from the fundamental frequency in the frequency-domain signal using the formula in Eq 19.

$$\mathrm{MOE_D} = \rho\left(2Lf_f\right)^2, \tag{19}$$

where f_f is the fundamental frequency.

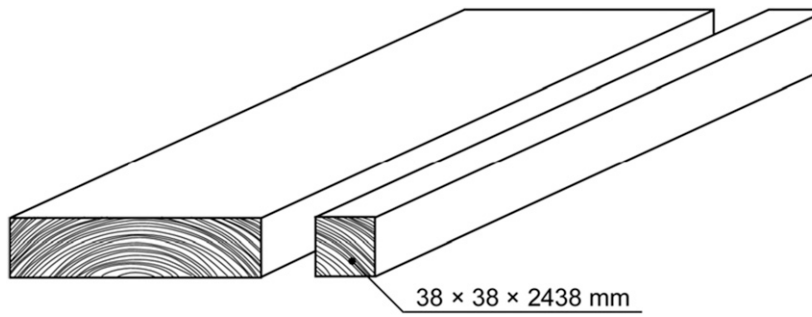

Figure 3. Time- and frequency-domain plots of a high- and low-elastic modulus specimen. The dashed vertical lines in the frequency-domain plots are the average fundamental frequency of 1030 Hz (Coefficient of Variation 10.2%) for all 103 specimens, and the first two harmonics at 2060 Hz and 3090 Hz. (a) and (c) are the time- and frequency-domain plots of defect-free specimen 74 with MOE of 11.6 GPA, respectively. (b) and (d) are the time- and frequency-domain plots of specimen 62 with MOE of 20.2 GPa, respectively.

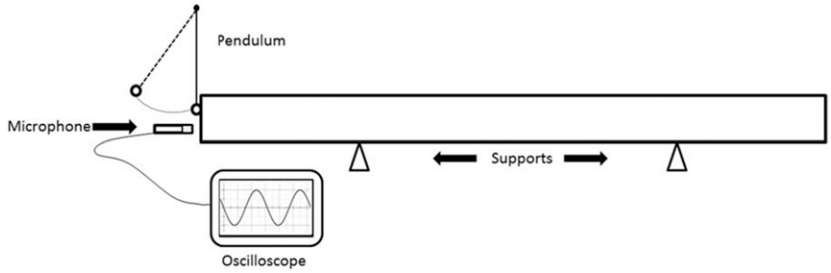

Figure 4. Unrestrained prismatic bar.

The primary sensing element is a commercially available microphone and condenser (microphone USB 2.0 and condenser SF-555B, with a frequency response range of 100 Hz-16 KHz and a sensitivity of -47 ± 4 dB). This is coupled to an IBM compatible laptop personal computer (Dell Model Latitude E6540, Round Rock, TX). Software from the Fakopp Portable Lumber Grader (version 2.0) is used for data acquisition and waveform analysis (Fakopp 2005).

RESULTS AND DISCUSSION

A displacement vs time plot constructed using Eq 18 is shown in Fig 5(a). Published values of MOE and specific gravities for loblolly pine from the *Wood Handbook* (Ross 2010) are used as inputs for the model. The attenuation value for the fundamental frequency, α_0, is calculated from McGovern et al (2013); the internal damping coefficient, $\bar{c}$, is calculated from α_0. The attenuation value for each harmonic is calculated using $\bar{c}$, the MOE, and the harmonic frequency. As a result, as harmonic frequency increases, attenuation increases. The signal is composed of the fundamental frequency and nine harmonics. The magnitude, D, is assigned a value of 1. With the passage of time, the harmonic components attenuate, leaving only the fundamental frequency. Visually, this transition is seen in Fig 5(a) as a shift from a skewed sinusoid at early time to an unskewed sinusoid later in the signal. In Fig 5(b), the frequency-domain plot of Fig 5(a) is shown. The fundamental frequency has the largest magnitude, with each subsequent harmonic having a decreasing magnitude.

The time-domain and frequency-domain plot for the signal collected from a wood specimen free of defects (specimen 74) is shown in Fig 6(a). The frequency-domain plot in Fig 6(c) is similar to the model plot shown in Fig 5(b). There is a distinct fundamental frequency and several prominent harmonics. Between the peaks, the plot is low magnitude and relatively flat. The differences between the time-domain signals of the model and specimen 74 are largely due to the phase angle of the individual frequencies. In the model

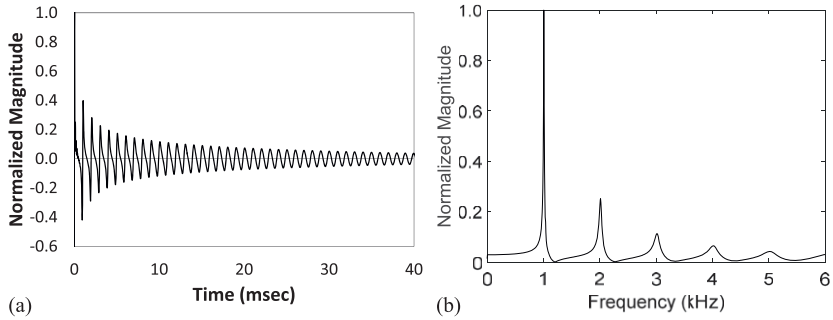

Figure 5. Free-body diagram of differential element dx.

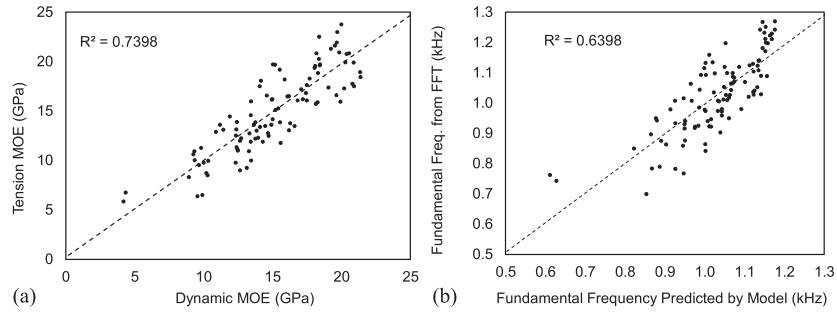

Figure 6. Construction of specimens.

(Fig 5[a]), all frequencies have an initial phase angle equal to zero. In the experimental setup (Fig 6 [a]), frequencies have nonzero initial phase angles, and the phase angles shifted slightly between frequencies. The difference is more noticeable early in the time-domain signal. Just as in the model, higher frequency harmonics attenuate more quickly, and eventually, only a few low-frequency components are left.

The diagrams in Fig 6 are a comparison of MOE and fundamental frequencies from acoustic wave measurement and static testing. In Fig 4(a), the dynamic MOE calculated using the fundamental frequency from the acoustic testing is compared against the MOE determined through tension tests of the same specimens. The r^2 value between the data sets is 0.74. Figure 6(b) shows the fundamental frequencies predicted by the model vs the fundamental frequencies taken from the fast Fourier transform of the signals recorded from each specimen. There is a linear relationship between the predicted values and the signal values with an r^2 value of 0.64. The two low points are confirmed as reliable values; however, if they are removed from the data set, the r^2 value is still 0.64. The model accounts for approximately 64% of the variation in the fundamental frequency and is a good starting point for analysis. Further refinement is necessary to accurately reflect the presence of defects.

Figure 7(b) shows the time-domain signal for specimen 62. The frequency domain for specimen

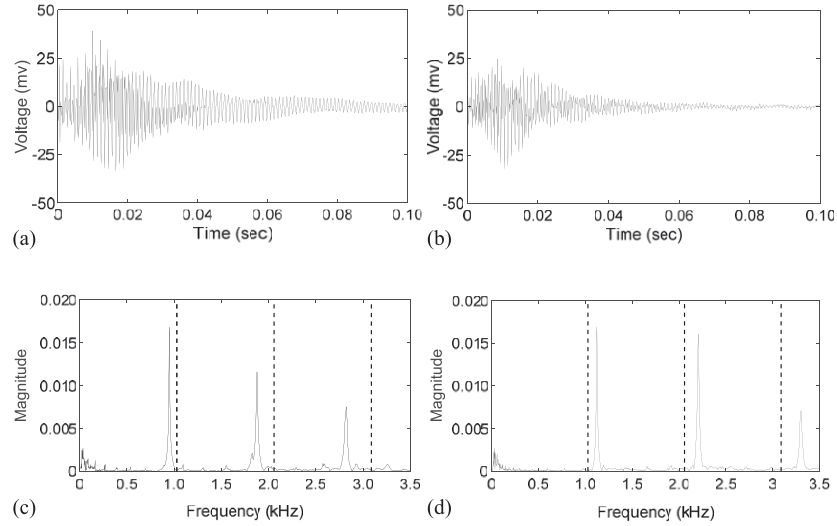

Figure 7. Experimental test setup recording time-domain signal.

62 is shown in Fig 7(d). The measured MOE values for specimen 74 (shown in Fig 7[c]) and specimen 62 (shown in Fig 7[d]) are 11.6 GPa and 20.2 GPa, respectively. The change in the fundamental frequency supports the known relationship between wave speed and MOE. For specimens of the same density, increasing longitudinal wave speed is indicative of higher stiffness. This relationship is described in Eq 9. The fundamental frequency increases directly with wave speed. As a result, higher fundamental frequencies are indicative of higher MOE values. The model presented in Eq 18 accurately reflects this relationship.

Future Work

The time- and frequency-domain curves contain a great deal of information that provides additional insights into the condition of the specimen. Figure 8(a) and (c) are, respectively, the time- and frequency-domain plots of specimen 74. Figure 8(b) and (d) are, respectively, the time- and frequency-domain plots of specimen 19. Specimen 74 is free of knots, slope of grain, or other defects. In the absence of any defects, the form of Fig 8(c) is similar to the form of the model in Fig 5(b). Both frequency-domain plots have distinct peaks but are mostly flat otherwise. Specimen 19 has a knot. The presence of the knot causes additional reflections of the stress wave. Figure 8(d) has a second peak slightly before the harmonic at 2 kHz. MOE_D is not altered by the presence of this second peak, but its existence indicates that a defect is present. Although it is clear that the fundamental frequency and harmonics are useful in characterizing wood, they are not the only information contained within the time and frequency domains. Examining the presence, magnitude, and location of other peaks may provide additional information about characteristics of the specimen that can improve the estimation of MOR and UTS.

CONCLUSIONS

The theoretical model developed in Part 1 of this research produces output similar to the testing of the experimental specimens. The model accounts for increasing attenuation with increasing frequency. The model allows for comparison between

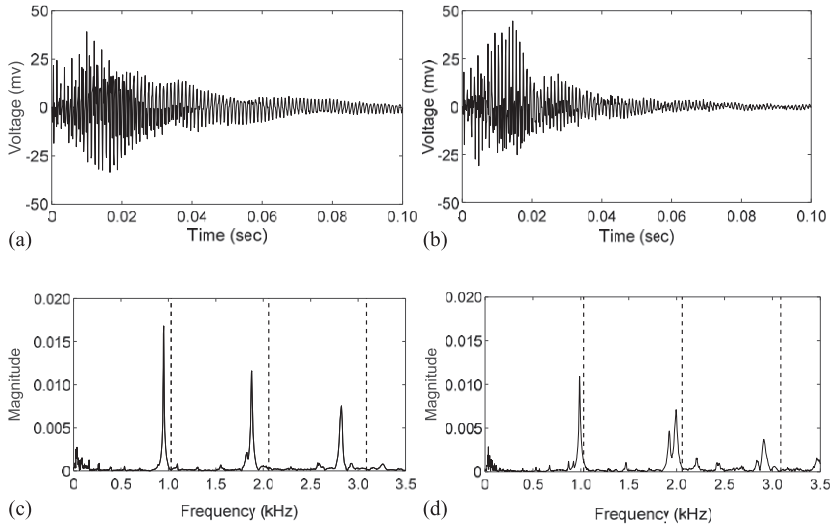

Figure 8. Time- and frequency-domain plots of a high- and low-elastic modulus specimen. The dashed vertical lines in the frequency-domain plots are the average fundamental frequency of 1030 Hz, and the first two harmonics at 2060 Hz and 3090 Hz. (a) and (c) are, respectively, the time- and frequency-domain plots of defect-free specimen 74 which failed in tension/shear. (b) and (d) are, respectively, the time- and frequency-domain plots of specimen 19 which failed in tension/shear in the area of a knot. Note the prominent second peak near 2 kHz.

ideal clear wood specimens and differences in time- and frequency-domain characteristics for specimens containing strength-reducing characteristics such as knots and slope of grain.

In Part 2 of this research, the model is used to help identify parameters that improve the estimation of UTS. Better estimations of UTS allow for higher usage from the wood resource.

REFERENCES

Bertholf LD (1965) Use of elementary stress wave theory for prediction of dynamic strain in wood. Washington State Institute of Technology, Bulletin 291. Washington State University, Pullman, WA. 86 pp.

Fakopp Enterprise (2005) Portable Lumber Grader software and hardware guide. Version 2.0, Ágfalva, Hungary. https://fakopp.com/docs/products/plg/PLGGuide.pdf.

Galligan WL, Bertholf LD (1963) Piezoelectric effect in wood. Forest Prod J 13:517-524.

Galligan WL, Courteau R (1965) Measurement of elasticity of lumber with longitudinal stress waves and the piezoelectric effect of wood. Pages 223-244 *in* WL Galligan, ed. Proc., 2nd Symposium Nondestructive Testing of Wood, April 1965, Spokane, WA. Washington State University, Pullman, WA.

Graff KE (1975) Wave motion in elastic solids. Dover Publications, Inc., New York, NY. 649 pp.

McGovern M, Senalik CA, Chen G, Beall FC, Reis H (2013) Effect of decay on ultrasonic velocity and attenuation measurements in wood. Mater Eval 71(10):1217-1231.

Pellerin RF, Galligan WL (1973) Nondestructive method of grading wood materials. Canadian Patent 918,286.

Ross RJ (1984) Stress wave speed and attenuation as predictors of the tensile and flexural properties of wood-based particle composites. PhD dissertation, Washington State University, Pullman, WA. 72 pp.

Ross RJ (2010) Wood handbook—Wood as an engineering material, Centennial edition. General Technical Report FPL-GTR-190. U.S. Department of Agriculture, Forest Service, Forest Products Laboratory, Madison, WI. 509 pp.

Ross RJ (2015) Nondestructive evaluation of wood, 2nd edition. General Technical Report FPL-GTR-238. U.S. Department of Agriculture, Forest Service, Forest Products Laboratory, Madison, WI. 176 pp.

Senalik CA (2013) Detection and assessment of wood decay–glulam beams and wooden utility poles. PhD dissertation, University of Illinois, Urbana-Champaign, IL. 232 pp.

Senalik CA, Schueneman G, Ross RJ (2014) Ultrasonic-based nondestructive evaluation methods for wood: A primer and historical review. General Technical Report FPL-GTR-235. U.S. Department of Agriculture, Forest Service, Forest Products Laboratory, Madison, WI. 36 pp.